Annals of Nuclear Medicine Vol. 17, No. 4, 289–295, 2003

Development of quantitative analysis method for stereotactic brain image: Assessment of reduced accumulation in extent and severity using anatomical segmentation

Sunao MIZUMURA, Shin-ichiro KUMITA, Keiichi CHO, Makiko ISHIHARA, Hidenobu NAKAJO, Masahiro TOBA and Tatsuo KUMAZAKI

Department of Radiology, Nippon Medical School

Through visual assessment by three-dimensional (3D) brain image analysis methods using stereotactic brain coordinates system, such as three-dimensional stereotactic surface projections and statistical parametric mapping, it is difficult to quantitatively assess anatomical information and the range of extent of an abnormal region. In this study, we devised a method to quantitatively assess local abnormal findings by segmenting a brain map according to anatomical structure. Through quantitative local abnormality assessment using this method, we studied the characteristics of distribution of reduced blood flow in cases with dementia of the Alzheimer type (DAT). Using twenty-five cases with DAT (mean age, 68.9 years old), all of whom were diagnosed as probable Alzheimer's disease based on NINCDS-ADRDA, we collected I-123 iodoamphetamine SPECT data. A 3D brain map using the 3D-SSP program was compared with the data of 20 cases in the control group, who age-matched the subject cases. To study local abnormalities on the 3D images, we divided the whole brain into 24 segments based on anatomical classification. We assessed the extent of an abnormal region in each segment (rate of the coordinates with a Z-value that exceeds the threshold value, in all coordinates within a segment), and severity (average Z-value of the coordinates with a Z-value that exceeds the threshold value). This method clarified orientation and expansion of reduced accumulation, through classifying stereotactic brain coordinates according to the anatomical structure. This method was considered useful for quantitatively grasping distribution abnormalities in the brain and changes in abnormality distribution.

Key words: three-dimensional stereotactic surface projections, I-123 iodoamphetamine, Talairach atlas, dementia with Alzheimer type

INTRODUCTION

AN ANALYSIS METHOD by region of interest (ROI) has been widely used as a conventional method to assess brain SPECT/PET images. However, the ROI analysis method has many problems, such as inadequate reproducibility and poor objectivity in analyzing lesions randomly selected by operators, and no capability to assess unknown pathology. 3D brain image analysis methods using stereotactic brain coordinates, such as three-dimensional stereotactic surface projections (3D-SSP)[1–3] and statistical parametric mapping (SPM)[4–6] are methods excellent in objectivity and reproducibility, due to automatic brain standardization and statistical processing of the whole brain, thus overcoming problems of the ROI method. These methods are excellent in abnormality detection in such functional diseases as dementia with Alzheimer type (DAT), and they are considered useful as diagnosis methods in many reports.[7–10] A three dimensional (3D) brain image analysis method presents statistically processed results as 3D coordinates and brain maps, making it easy to assess the spatial extent of an abnormal site. Brain mapping by a 3D brain image analysis method is assuredly an effective method to grasp the entire image of an

Received January 6, 2003, revision accepted March 6, 2003.

For reprint contact: Sunao Mizumura, M.D., Department of Radiology, Nippon Medical School, 1–1–5, Sendagi, Bunkyo-ku, Tokyo 115–8603, JAPAN.

E-mail: sunaom@nms.ac.jp

Table 1 Anatomical classification based on the Talairach Daemon database

Level 1	Level 3		Level 5	
Inter-Hemispheric	Angular Gyrus	Orbital Gyrus	Anterior Commissure	Brodmann area 32
Brainstem	Anterior Cingulate	Paracentral Lobule	Brodmann area 1	Brodmann area 33
Cerebellum	Cerebellar Lingual	Parahippocampal Gyrus	Brodmann area 2	Brodmann area 34
Cerebrum	Cerebellar Tonsil	Postcentral Gyrus	Brodmann area 3	Brodmann area 35
	Cingulate Gyrus	Posterior Cingulate	Brodmann area 4	Brodmann area 36
Level 2	Culmen	Precentral Gyrus	Brodmann area 5	Brodmann area 37
Anterior Lobe	Culmen of Vermis	Precuneus	Brodmann area 6	Brodmann area 38
Frontal Lobe	Cuneus	Pyramis	Brodmann area 7	Brodmann area 39
Frontal-Temporal Space	Declive	Pyramis of Vermis	Brodmann area 8	Brodmann area 40
Limbic Lobe	Declive of Vermis	Rectal Gyrus	Brodmann area 9	Brodmann area 42
Medulla	Extra-Nuclear	Subcallosal Gyrus	Brodmann area 10	Brodmann area 43
Midbrain	Fourth Ventricle	Sub-Gyral	Brodmann area 11	Brodmann area 44
Occipital Lobe	Fusiform Gyrus	Superior Frontal Gyrus	Brodmann area 17	Brodmann area 45
Parietal Lobe	Inferior Frontal Gyrus	Superior Occipital Gyrus	Brodmann area 18	Brodmann area 46
Pons	Inferior Occipital Gyrus	Superior Parietal Lobule	Brodmann area 19	Brodmann area 47
Posterior Lobe	Inferior Parietal Lobule	Superior Temporal Gyrus	Brodmann area 20	Corpus Callosum
Sub-lobar	Inferior Semi-lunar Lobule	Supramarginal Gyrus	Brodmann area 21	Mammillary Body
Temporal Lobe	Inferior Temporal Gyrus	Thalamus	Brodmann area 22	Medial Dorsal Nucleus
	Lateral Ventricle	Third Ventricle	Brodmann area 23	Optic Tract
Level 4	Lingual Gyrus	Transverse Temporal Gyrus	Brodmann area 24	
Cerebro-spinal Fluid	Medial Frontal Gyrus	Tuber	Brodmann area 25	
Gray Matter	Middle Frontal Gyrus	Tuber of Vermis	Brodmann area 28	
White Matter	Middle Occipital Gyrus	Uncus	Brodmann area 29	
	Middle Temporal Gyrus	Uvula	Brodmann area 30	
	Nodule	Uvula of Vermis	Brodmann area 31	

Five types of classification are set up according to respective anatomical structures. Extent and severity of each region can be calculated regardless of which classification is used.

abnormal region, but it is difficult to clearly indicate anatomical information of an abnormal site in visual assessment of 3D images. Therefore, topography at the boundary of an abnormal area cannot be specifically shown, making it impossible to quantitatively assess the extent of a lesion. In this situation, it is not a good choice to perform ROI analysis of a brain map based on the statistical results, to study local abnormal findings, because artificial setting of ROI will result in loss of objectivity and reproducibility of analysis results, and evaluation without classification between an abnormal and a normal region.

We devised a quantitative evaluation method, using the extent and severity indices of lesion in the whole brain or in the brain structure related to pathology. We classified a brain surface display into segments according to the anatomical structure, and prepared indices to assess the extent and severity of lesion in respective segments, in order to quantitatively identify an abnormal area according to a 3D brain image analysis method. In this study, we show the results of this analysis method in DAT cases.

SUBJECTS AND METHODS

We studied twenty-five cases with DAT (mean age ± s.d., 68.9 ± 7.2), all of which were diagnosed as probable Alzheimer's disease based on NINCDS-ADRDA.[11] As a control group, we used 20 cases, age-matched with the subjects, and showed only changes due to aging in white matter in MRI and no abnormal neurological findings.

Data acquisition

We administered intravenous injection of I-123 iodoamphetamine 222 MBq to the subjects, at rest, with their eyes closed while in the supine position. We performed SPECT data collection (3 sec/step, 72 steps, 5 repeats) for about 30 minutes, starting at 25 minutes after intravenous injection. The matrix size was 128 × 128, and the collection window was 160 keV, at 20%. For prefilter and absorption correction, the Ramp-Butterworth filter (order 5, cutoff 0.26) and the Radial Post-correction method, were used, and images were reconstructed using the back-projection method. The image voxel size was 2 × 2 × 5 mm. The SPECT system used was a ring-type gamma camera (SET-080; Shimadzu Co., Kyoto, Japan) with a general-purpose fan-beam collimator (FWHM 12 mm).

We normalized the obtained transverse images of the twenty subjects and the control group, and created brain map data using the 3D-SSP program. Next, we prepared Z-value surface data by conducting statistical processing of the subject group (Student's unpaired-t testing) or a case (Jackknife testing), regarding the obtained brain map data.

Segmentation based on the anatomical classification of a brain map

We conducted data conversion to make 15,965 coordinate data, of which the 3D-SSP brain map consist, conform to the Talairach brain atlas.[12] We obtained anatomical information in respective brain coordinates, using the Talairach Daemon (Research Imaging Center, University of Texas Laboratory)[13–15] for the coordinate data obtained after the conversion.

We prepared a reference table in which the obtained brain coordinates correspond to anatomical information, and conducted Z-value association between the coordinates in the prepared reference table and the case coordinates. Subsequently, we calculated a total of coordinate

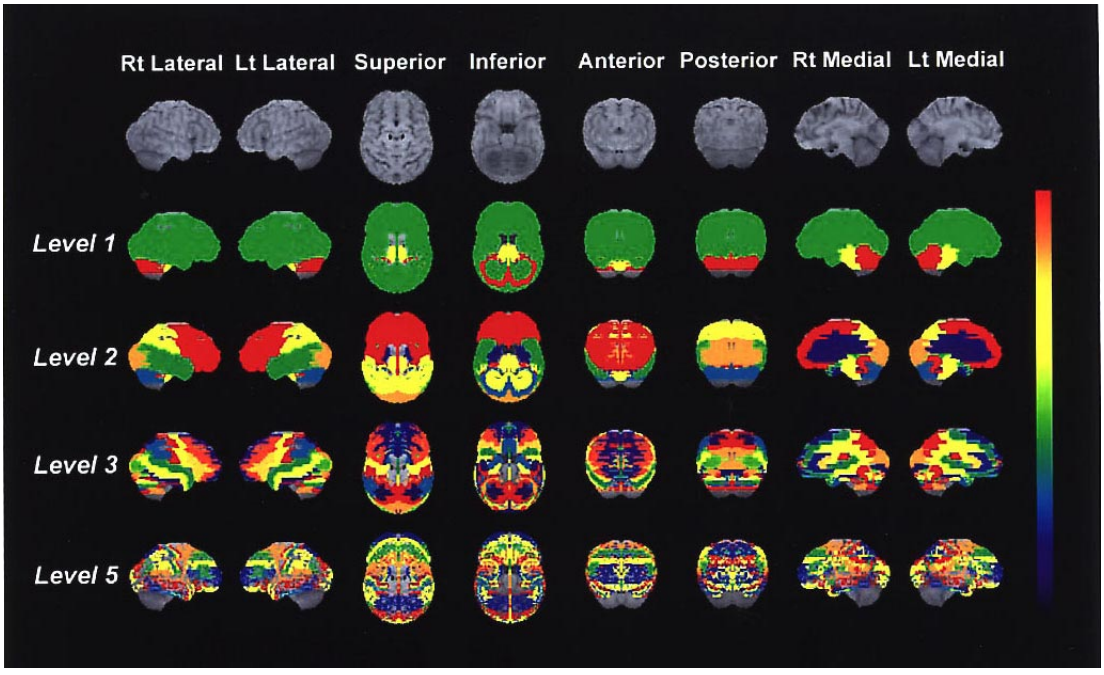

Fig. 1 Brain surface images, color-coded in six colors, and anatomically classified in four types. Brain surface images, classified by four levels, out of five levels, except for Level 4 (classification of gray matter and white matter), were color-coded in six colors. From the top, brain surface images classified by Level 1, Level 2, Level 3, and Level 5 are shown. As to the Level 5 Brodmann Area classification, each segment consists of a small number of coordinates, and contiguous segments could not be well separated on the display, but on the classification display of Level 1 to 3, anatomically structural separation was confirmed. In the Talairach Daemon brain coordinates, information on the upper border of the vertex and the lower border of the cerebellum is lacking.

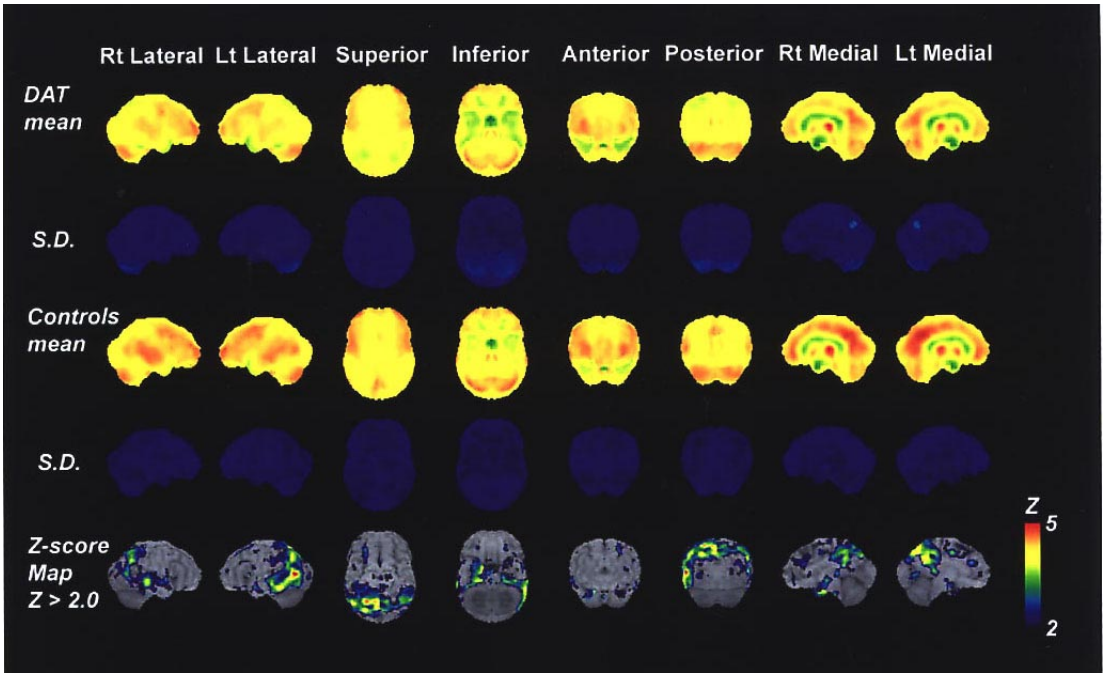

Fig. 2 Z-score map of comparison between the group of DAT cases and the group of control cases. From the top, brain surface images of mean image and standard deviation image in DAT, brain surface images of mean image and standard deviation image in control group, Z-score map on unpaired t-test are shown. Compared with the control group, the Z-score map of the group of the DAT cases showed decreased accumulation in the posterior cingulate gyrus and vertex cortex.

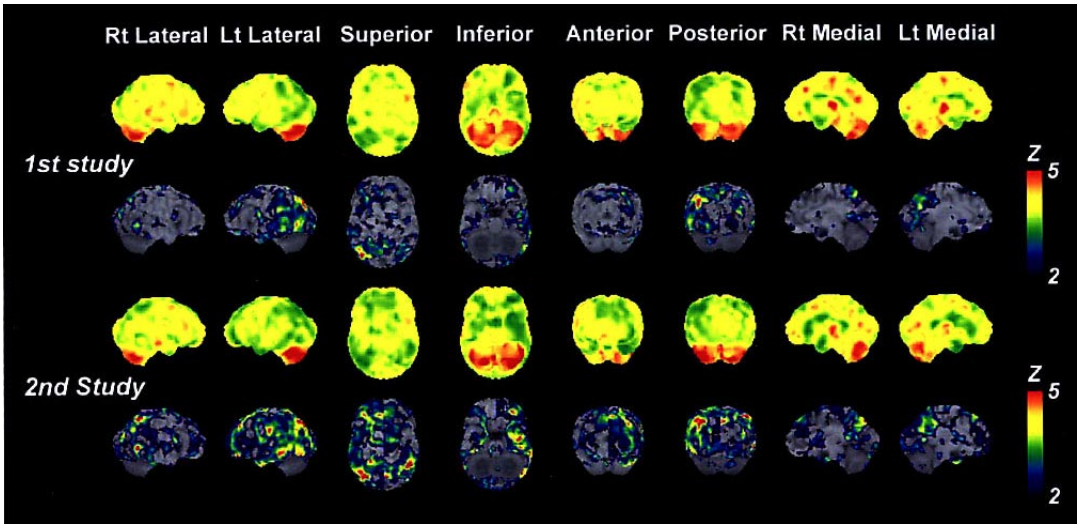

Fig. 3 Z-score map of comparison between the group of DAT cases and the group of control cases. From the top, mean images and Z-score map on first study, mean images and Z-score map on second study are shown. In the Z-score map at the initial test, decreased accumulation was noted in the parietal cortex, temple cortex, and posterior cingulate gyrus. The Z-score map at the test six months later showed expansion of lowered blood flow to the frontal cortex.

Table 2 Abstract from the SEE method results on brain maps of the group of DAT cases and the group of control cases, and on Level 2 and 3 (lobe and gyrus level classification)

Level 2

area			extent		mean	SD	area			extent		mean	SD	area			extent		mean	SD
Frontal Lobe	Left	2244	14.1%	316	2.35	0.33	Temporal Lobe	Left	882	62.4%	550	2.95	0.63	Limbic Lobe	Left	654	43.3%	283	2.82	0.60
	Right	2255	8.7%	196	2.34	0.32		Right	877	56.2%	493	2.52	0.43		Right	651	50.5%	329	2.82	2.82
Parietal Lobe	Left	893	77.9%	696	3.16	0.67	Occipital Lobe	Left	712	33.1%	236	2.74	0.60							
	Right	890	56.9%	506	2.84	2.84		Right	715	11.6%	83	2.38	0.32							

Level 3

	area			extent		mean	SD		area			extent		mean	SD		area			extent		mean	SD
Frontal Lobe	Superior Frontal	Left	548	11.1%	61	2.32	2.32	Parietal Lobe	Superior Parietal Lobule	Left	120	99.2%	119	3.49	0.59	Occipital Lobe	Superior Occipital Gyrus	Left	23	47.8%	11	2.26	0.22
		Right	555	1.1%	6	2.32	2.32			Right	120	74.2%	89	2.76	0.48			Right	22	90.9%	20	2.40	0.18
	Middle Frontal	Left	547	12.8%	70	2.32	0.25		Inferior Parietal Lobule	Left	190	75.8%	144	2.71	0.57		Middle Occipital Gyrus	Left	160	57.5%	92	2.88	0.69
		Right	547	1.5%	8	2.21	0.10			Right	188	69.7%	131	2.82	0.39			Right	159	25.8%	41	2.25	0.22
	Inferior Frontal	Left	300	6.7%	20	2.17	0.14		Angular Gyrus	Left	20	100.0%	20	3.45	0.51		Inferior Occipital Gyrus	Left	50	14.0%	7	2.40	0.26
		Right	297	3.7%	11	2.29	0.20			Right	20	65.0%	13	2.89	0.66			Right	49	0.0%	0	Null	Null
	Medial Frontal	Left	366	19.1%	70	2.21	0.19		Postcentral Gyrus	Left	239	48.1%	115	2.54	0.31		Cuneus	Left	303	27.1%	82	2.51	0.29
		Right	363	22.6%	82	2.20	0.13			Right	237	13.1%	31	2.26	0.19			Right	306	2.0%	6	2.33	0.39
	Orbital Gyrus	Left	20	0.0%	0	Null	Null		Precuneus	Left	314	88.2%	277	3.50	0.56		Fusiform Gyrus	Left	88	62.5%	55	2.92	0.40
		Right	22	0.0%	0	Null	Null			Right	314	68.8%	216	2.96	0.42			Right	88	13.6%	12	2.37	2.37
	Rectal Gyrus	Left	64	0.0%	0	Null	Null		Supramarginal Gyrus	Left	43	90.7%	39	2.85	0.46		Lingual Gyrus	Left	99	8.1%	8	2.52	0.35
		Right	64	10.9%	7	2.07	0.05			Right	44	54.5%	24	2.92	0.64			Right	100	0.0%	0	Null	Null
	Paracentral Lobule	Left	85	72.9%	62	2.71	0.41	Temporal Lobe	Inferior Semi-lunar Lobule	Left	71	0.0%	0	Null	Null		Cingulate Gyrus	Left	267	58.4%	156	2.93	2.93
		Right	85	71.8%	61	2.63	0.40			Right	71	0.0%	0	Null	Null			Right	267	55.1%	147	2.71	2.71
	Precentral Gyrus	Left	224	5.8%	13	2.18	0.16		Superior Temporal Gyrus	Left	306	52.0%	159	2.59	2.59		Parahippocampal Gyrus	Left	43	95.3%	41	2.80	0.46
		Right	225	3.1%	7	2.16	0.15			Right	304	58.2%	177	2.44	2.44			Right	43	93.0%	40	3.20	0.60
	Subcallosal Gyrus	Left	20	5.0%	1	2.07	Null		Middle Temporal Gyrus	Left	341	78.0%	266	3.11	0.69		Anterior Cingulate	Left	180	12.8%	23	2.51	0.32
		Right	20	5.0%	1	2.35	Null			Right	345	72.2%	249	2.65	0.50			Right	180	17.2%	31	2.37	0.25
	Thalamus	Left	8	0.0%	0	Null	Null		Inferior Temporal Gyrus	Left	157	51.0%	80	3.35	0.53		Posterior Cingulate	Left	98	40.8%	40	3.02	0.49
		Right	8	0.0%	0	Null	Null			Right	154	35.1%	54	2.30	0.20			Right	98	46.9%	46	2.57	0.55
									Transverse Temporal Gyrus	Left	6	0.0%	0	Null	Null		Uncus	Left	79	46.8%	37	2.14	0.11
										Right	6	66.7%	4	2.16	0.10			Right	79	93.7%	74	3.10	0.49

In each row, anatomical information, total coordinates, rate of abnormal coordinates in total coordinates, total coordinates of abnormalities, mean of abnormalities, and standard deviation of abnormalities are presented from the left. In the SEE method results, these characteristics of the images demonstrate a similar blood flow abnormality region to brain maps, also in comparison between the groups.

data with a Z-value that exceeds the threshold of the Z-value set as a significant finding; the rate of the total coordinates with significantly reduced Z-value in the total of coordinates in respective segments (extent), and the average and the standard deviation of coordinates with significantly reduced Z-value (severity). We prepared a table by combining the indices according to segments and anatomical classification, and we assessed any significant decrease of accumulation (stereotactic extraction estimation method; SEE method).

Table 3 Abstract from the SEE method results on brain maps in the initial test, and the six-month later test, in DAT cases, and on Level 2 and 3 (lobe and gyrus level classification)

1st Study

Level 2

area			extent		mean	SD	area			extent		mean	SD	area			extent		mean	SD
Frontal Lobe	Left	2244	34.7%	778	2.43	0.38	Temporal Lobe	Left	882	76.5%	675	2.77	0.51	Limbic Lobe	Left	654	28.1%	184	2.47	0.43
	Right	2255	14.9%	336	2.30	0.28		Right	877	23.3%	204	2.46	0.43		Right	651	16.0%	104	2.43	2.43
Parietal Lobe	Left	893	80.4%	718	2.90	0.65	Occipital Lobe	Left	712	61.1%	435	2.72	0.57							
	Right	890	43.9%	391	2.64	2.64		Right	715	40.4%	289	2.41	0.43							

Level 3

	area			extent		mean	SD	area			extent		mean	SD	area			extent		mean	SD
Frontal Lobe	Superior Frontal	Left	548	48.7%	267	2.42	2.42	Parietal Lobe	Superior Parietal	Left	120	98.3%	118	3.02	0.50	Occipital Lobe	Superior Occipital	Left	23	95.7%	22	3.65	0.88
	Gyrus	Right	555	18.7%	104	2.42	2.42		Lobule	Right	120	70.0%	84	2.83	0.36		Gyrus	Right	22	100.0%	22	2.95	0.42
	Middle Frontal	Left	547	48.6%	266	2.51	0.37		Inferior Parietal	Left	190	74.2%	141	3.01	0.66		Middle Occipital	Left	160	79.4%	127	2.79	0.57
	Gyrus	Right	547	9.7%	53	2.23	0.18		Lobule	Right	188	34.6%	65	2.46	0.42		Gyrus	Right	159	46.5%	74	2.57	0.61
	Inferior Frontal	Left	300	19.3%	58	2.47	0.51		Angular Gyrus	Left	20	100.0%	20	3.38	0.71		Inferior Occipital	Left	50	66.0%	33	2.59	0.51
	Gyrus	Right	297	19.5%	58	2.46	0.35			Right	20	45.0%	9	2.28	0.19		Gyrus	Right	49	46.9%	23	2.22	0.12
	Medial Frontal	Left	366	14.2%	52	2.24	0.20		Postcentral Gyrus	Left	239	53.6%	128	2.40	0.35		Cuneus	Left	303	35.6%	108	2.46	0.37
	Gyrus	Right	363	8.3%	30	2.12	0.08			Right	237	15.2%	36	2.48	0.30			Right	306	42.8%	131	2.34	0.26
	Orbital Gyrus	Left	20	75.0%	15	2.15	0.08		Precuneus	Left	314	94.6%	297	3.02	0.71		Fusiform Gyrus	Left	88	84.1%	74	2.77	0.48
		Right	22	0.0%	0	Null	Null			Right	314	63.4%	199	2.66	0.49			Right	88	50.0%	44	2.30	2.30
	Rectal Gyrus	Left	64	12.5%	8	2.11	0.05		Supramarginal	Left	43	95.3%	41	2.78	0.48		Lingual Gyrus	Left	99	74.7%	74	2.57	0.37
		Right	64	17.2%	11	2.10	0.10		Gyrus	Right	44	4.5%	2	2.72	0.31			Right	100	20.0%	20	2.15	0.11
	Paracentral Lobule	Left	85	17.6%	15	2.25	0.16	Temporal Lobe	Inferior Semi-lunar	Left	71	22.5%	16	2.62	0.35		Cingulate Gyrus	Left	267	25.5%	68	2.57	2.57
		Right	85	30.6%	26	2.52	0.28		Lobule	Right	71	0.0%	0	Null	Null			Right	267	1.5%	4	2.35	2.35
	Precentral Gyrus	Left	224	33.5%	75	2.39	0.42		Superior Temporal	Left	306	60.5%	185	2.58	2.58		Parahippocampal	Left	43	51.2%	22	2.36	0.24
		Right	225	16.9%	38	2.29	0.25		Gyrus	Right	304	11.5%	35	2.16	2.16		Gyrus	Right	43	16.3%	7	2.50	0.32
	Subcallosal Gyrus	Left	20	45.0%	9	2.45	0.22		Middle Temporal	Left	341	88.9%	303	2.91	0.46		Anterior Cingulate	Left	180	7.8%	14	2.12	0.12
		Right	20	25.0%	5	2.11	0.08		Gyrus	Right	345	21.4%	74	2.66	0.50			Right	180	2.2%	4	2.20	0.08
	Thalamus	Left	8	0.0%	0	Null	Null		Inferior Temporal	Left	157	87.3%	137	2.76	0.59		Posterior Cingulate	Left	98	49.0%	48	2.57	0.51
		Right	8	0.0%	0	Null	Null		Gyrus	Right	154	40.9%	63	2.45	0.38			Right	98	41.8%	41	2.55	0.36
									Transverse Temporal	Left	6	16.7%	1	2.10	Null		Uncus	Left	79	39.2%	31	2.33	0.24
									Gyrus	Right	6	16.7%	1	2.03	Null			Right	79	59.5%	47	2.32	0.20

2nd Study

Level 2

area			extent		mean	SD	area			extent		mean	SD	area			extent		mean	SD
Frontal Lobe	Left	2244	74.1%	1662	2.70	0.60	Temporal Lobe	Left	882	91.4%	806	3.19	0.70	Limbic Lobe	Left	654	56.3%	368	2.76	0.66
	Right	2255	47.6%	1074	2.48	0.39		Right	877	58.2%	510	2.66	0.67		Right	651	46.5%	303	2.58	2.58
Parietal Lobe	Left	893	92.0%	822	3.12	0.73	Occipital Lobe	Left	712	85.8%	611	2.70	0.55							
	Right	890	82.1%	731	3.00	3.00		Right	715	50.9%	364	2.51	0.38							

Level 3

	area			extent		mean	SD	area			extent		mean	SD	area			extent		mean	SD
Frontal Lobe	Superior Frontal	Left	548	88.1%	483	2.78	2.78	Parietal Lobe	Superior Parietal	Left	120	100.0%	120	3.47	0.77	Occipital Lobe	Superior Occipital	Left	23	95.7%	22	3.35	0.85
	Gyrus	Right	555	52.3%	290	2.78	2.78		Lobule	Right	120	97.5%	117	3.15	0.66		Gyrus	Right	22	54.5%	12	2.76	0.60
	Middle Frontal	Left	547	85.4%	467	2.83	0.63		Inferior Parietal	Left	190	98.9%	188	3.05	0.68		Middle Occipital	Left	160	89.4%	143	2.98	0.68
	Gyrus	Right	547	53.6%	293	2.48	0.35		Lobule	Right	188	97.9%	184	3.17	0.99		Gyrus	Right	159	59.7%	95	2.49	0.45
	Inferior Frontal	Left	300	81.3%	244	2.57	0.47		Angular Gyrus	Left	20	100.0%	20	3.85	0.50		Inferior Occipital	Left	50	82.0%	41	2.62	0.38
	Gyrus	Right	297	47.1%	140	2.58	0.52			Right	20	100.0%	20	3.35	0.49		Gyrus	Right	49	79.6%	39	2.52	0.23
	Medial Frontal	Left	366	51.9%	190	2.29	0.22		Postcentral Gyrus	Left	239	84.9%	203	3.10	0.72		Cuneus	Left	303	84.5%	256	2.48	0.36
	Gyrus	Right	363	47.7%	173	2.36	0.25			Right	237	52.3%	124	2.42	0.25			Right	306	35.0%	107	2.39	0.31
	Orbital Gyrus	Left	20	100.0%	20	2.27	0.25		Precuneus	Left	314	87.6%	275	2.98	0.72		Fusiform Gyrus	Left	88	83.0%	73	3.27	0.73
		Right	22	0.0%	0	Null	Null			Right	314	88.9%	279	3.11	0.65			Right	88	65.9%	58	2.78	2.78
	Rectal Gyrus	Left	64	12.5%	8	2.24	0.14		Supramarginal	Left	43	102.3%	44	3.07	0.51		Lingual Gyrus	Left	99	77.8%	77	2.69	0.32
		Right	64	9.4%	6	2.11	0.05		Gyrus	Right	44	81.8%	36	2.44	0.42			Right	100	63.0%	63	2.52	0.32
	Paracentral Lobule	Left	85	47.1%	40	2.59	0.40	Temporal Lobe	Inferior Semi-lunar	Left	71	15.5%	11	2.39	0.31		Cingulate Gyrus	Left	267	50.2%	134	2.72	2.72
		Right	85	57.6%	49	2.25	0.18		Lobule	Right	71	32.4%	23	2.60	0.28			Right	267	27.0%	72	2.38	2.38
	Precentral Gyrus	Left	224	73.7%	165	2.97	0.68		Superior Temporal	Left	306	85.3%	261	2.82	2.82		Parahippocampal	Left	43	79.1%	34	2.59	0.37
		Right	225	43.6%	98	2.35	0.29		Gyrus	Right	304	52.6%	160	2.38	2.38		Gyrus	Right	43	60.5%	26	2.89	0.80
	Subcallosal Gyrus	Left	20	25.0%	5	2.14	0.12		Middle Temporal	Left	341	98.2%	335	3.31	0.72		Anterior Cingulate	Left	180	33.9%	61	2.22	0.17
		Right	20	0.0%	0	Null	Null		Gyrus	Right	345	66.1%	228	2.82	0.78			Right	180	33.3%	60	2.22	0.16
	Thalamus	Left	8	0.0%	0	Null	Null		Inferior Temporal	Left	157	94.9%	149	3.42	0.68		Posterior Cingulate	Left	98	69.4%	68	2.97	0.58
		Right	8	0.0%	0	Null	Null		Gyrus	Right	154	45.5%	70	2.73	0.71			Right	98	80.6%	79	2.71	0.40
									Transverse Temporal	Left	6	50.0%	3	2.59	0.41		Uncus	Left	79	88.6%	70	3.19	0.73
									Gyrus	Right	6	50.0%	3	2.22	0.15			Right	79	91.1%	72	2.75	0.57

According to the analysis results classified by lobe level, extent of reduced accumulation in the parietal cortex and temple cortex was 80.4 to 92.0%, 76.5 to 91.4% on the left and 43.9 to 82.1%, 23.3 to 58.2% on the right, respectively. On the other hand, the reduced accumulation region expanded from 34.7 to 74.1% and 14.9 to 47.6% of the frontal cortex, and quantitative assessment indicated similar results to findings in brain surface images. In general, in ischemic diseases, expansion of the reduced blood flow region results in marked level of lowering of local blood flow. However, in functional diseases, increased severity was seldom seen, indicating that lesion expansion and severity of local disorder are not directly related.

RESULTS

According to the Talairach Daemon, anatomical information is segmented into five levels from 1 to 5: the hemisphere, lobe, gyrus, cortex/white matter, and Brodmann Area levels (Table 1 and Fig. 1). Further, information on the right side and the left side was classified only in level 1, so the classification of left and right was added to each level. As a result, respective levels were classified into 7, 100, 24, 6, and 88. The numbers of coordinates where anatomical information was obtained by classification of levels 1 to 5, out of the 15,965 coordinate data on the 3D-SSP surface map, were 13,557 (84.9%), 13,370 (83.7%), 12,603 (78.9%), 9,006 (56.4%), and 6,148 (38.5%). In the classification of Level 5: Brodmann Area, as it is originally part of the brain surface, data account for 40% or below of all brain surface coordinates. According to other classifications, coordinates in which anatomical information could be obtained were 55 to 85% of all the brain surface coordinates, as Talairach Daemon data do not contain data on the upper border of the vertex and the lower border of the cerebellum, and there were other

regions besides brain parenchyma, such as the sulcus of the brain.

We show the results of comparison between DAT cases and the control groups (Table 2 and Fig. 3). It is easy to recognize spatial extent regarding the results of brain maps when DAT cases were compared with the control groups. However, quantitative and anatomical assessment of the difference is inadequate. SEE method enables direct comparison of differences in extent and severity according to segments, between the two groups. As such, it is understood that this method not only enables grasping and quantification of regions but also facilitates comparative study.

This method enables assessment also when changes over time in one case are compared. We show the results of this analysis in DAT cases from which data were collected twice (Table 3 and Fig. 3). Visually also, changes in the regions of abnormal blood flow can be confirmed, but SEE method quantified the extent and severity of the specific regions with an abnormality in blood flow. When changes over time in one case are compared, one image and another are compared, so it is not possible to statistically compare the change between the two images. On the other hand, SEE method can quantify the results of statistical comparison with the control group, so changes in blood flow distribution can be obtained from the difference in extent and severity between the two brain maps.

DISCUSSION

For group comparisons, Student's unpaired t-test and paired t-test are generally used. 3D brain image analysis methods, such as 3D-SSP and SPM, enable extremely easy spatial recognition, as they indicate the extent of abnormal regions on a brain map. While SPM aims to indicate foci with a significant difference over the whole brain, for activation test analysis, 3D-SSP has a clinical purpose of diagnosing by detecting distribution forms of abnormal regions in the brain. These analysis methods have respective characteristics, and statistical results are only displayed in images and brain coordinates for their original purpose. In 3D mapping of the results of statistical processing by Student's t-test and Jackknife test, anatomical identification and comparison of the extent of abnormal regions by only visual assessment are difficult. In these analysis methods, quantitative assessment is not conducted sufficiently, with their latent potential being hidden. To reflect anatomical information and indicate the extent of a clearly abnormal regions, a method that supplements such brain mapping is desired. The analysis method we devised digitalizes local abnormalities on a table, immediately from classification based on the anatomical structure, enabling easy assessment. Consequently, our method required strict normalization of brain images, and quality control of the normalized image obtained by 3D-SSP is needed. Once quality control can be checked, we expect the method to expand the possibilities of the 3D brain image analysis method. Even in the case of "follow-up on a single case in which group testing is not possible," it is possible to compare two images by assessing the abnormal region by SEE method, using the results of the Jackknife testing, obtained by comparison with the control group. The method has a possibility of yielding indices for comparison of intra-subjects, which could not be statistically compared. The decisive difference between the conventionally used ROI method and this method, is that the ROI method is an analysis on a lesion site that a technician randomly selects, while this method enables analysis by selectively extracting a site judged as being abnormal based on statistical results. With this method, therefore, an abnormal site and a normal site can be clearly distinguished.

Consideration for such accurate data extraction is seen also in 3D-SSP.[16] Accumulation evaluation on brain cortex by the voxel of interest (VOI) method cannot avoid underestimation caused by partial volume effect. In 3D-SSP, data extract, which avoids influence due to partial volume effect, is conducted by extracting the maximum value of brain cortex data in the direction from the brain surface tangentially. These data extract methods can be said to be innovative data analysis methods to eliminate errors caused by the classic ROI or VOI method, though their purposes are different.

Further, our analysis methods aim to grasp an abnormal region over the whole image by tallying the abnormal sites in clinically significant regions, through classification according to anatomical structure beforehand. In particular, this method emphasizes on the concept of extent, so analysis is conducted aiming to effectively assess extent of an abnormal blood flow region. To assess functional diseases, such as dementia, we think studying the extent of the region of abnormal blood flow that causes functional disorder is more rational than assessing the severity of the blood flow abnormality that reflects local tissue degeneration. The anatomical classification we used in this study cannot be said to be adequate to investigate foci by brain activation testing, but for assessing lesion extent, it is expected to be useful. Even with SPM volume data, having the same concept on extent of an abnormal region, this analysis method can be applied. However, when anatomical classification is considered, the number of segments to classify will be huge in volume data analysis. Processing data tends to be complicated, easily causing errors, so it is desirable, also from the viewpoint of versatility, not to increase data without good reason. Rather, use for information for a projection table, like a brain map, is considered more effective as clinical usage. In the Talairach Daemon, brain anatomy is classified into levels 1 to 5. Images with high resolution, such as MRI and PET, can maintain reliability toward analysis results even if detailed anatomical classification is conducted. However, with a SPECT system, with low resolu-

tion of about 10 mm in full width half maximum, data reliability cannot be expected in the most detailed classification, such as of Brodmann Area. In other words, in analysis using this method in SPECT, the region classification from the lobe level to the gyrus level will be appropriate, but it is considered necessary to study the limit of division analysis according to resolution of image collection systems.

CONCLUSION

We classified brain coordinates into segments based on brain anatomy, and devised a method to quantitatively assess brain image abnormalities, based on numerical indices in extent and severity, and anatomical information on a brain map.

REFERENCES

1. Minoshima S, Koeppe RA, Frey KA, Ishihara M, Kuhl DE. Stereotactic PET atlas of the human brain: aid for visual interpretation of functional brain images. *J Nucl Med* 1994; 35: 949–954.
2. Minoshima S, Foster NL, Kuhl DE. Posterior cingulate cortex in Alzheimer's disease. *Lancet* 1994; 24, 344 (8926): 895
3. Minoshima S, Frey KA, Koeppe RA, Foster NL, Kuhl DE. A diagnostic approach in Alzheimer's disease using three-dimensional stereotactic surface projections of fluorine-18-FDG PET. *J Nucl Med* 1995; 36: 1238–1248.
4. Friston KJ, Frith CD, Liddle PF, Dolan RJ, Lammertsma AA, Frackowiak RSJ. The relationship between global and local changes in PET scans. *J Cereb Blood Flow Metab* 1990; 10: 458–466.
5. Friston KJ, Frith CD, Liddle PF, Frackowiak RSJ. Comparing functional (PET) images: The assessment of significant change. *J Cereb Blood Flow Metab* 1991; 11: 690–699.
6. Frith CD, Friston KJ, Ashburner J, Holmes A, Poline J, Worsley K, et al. Principles and methods. In: Frackowiak RSJ, Friston KJ, Frith CD, Dolan RJ, Mazziotta JC (eds), *Human Brain Function*. San Diego; Accademic Press, 1997: 3–159.
7. Burdette JH, Minoshima S, Vander Borght T, Tran DD, Kuhl DE. Alzheimer disease: improved visual interpretation of PET images by using three-dimensional stereotaxic surface projections. *Radiology* 1996; 198: 837–843.
8. Sakamoto S, Ishii K, Sasaki M, Hosaka K, Mori T, Matsui M, et al. Differences in cerebral metabolic impairment between early and late onset types of Alzheimer's disease. *J Neurol Sci* 2002; 15 (200): 27–32.
9. Matsuda H. Cerebral blood flow and metabolic abnormalities in Alzheimer's disease. *Ann Nucl Med* 2001; 15: 85–92.
10. Kogure D, Matsuda H, Ohnishi T, Asada T, Uno M, Kunihiro T, et al. Longitudinal evaluation of early Alzheimer's disease using brain perfusion SPECT. *J Nucl Med* 2000; 41: 1155–1162.
11. McKhann G, Drachman D, Folstein M, Katzman R, Price D, Stadlan EM. Clinical diagnosis of Alzheimer's disease: report of the NINCDS-ADRDA Work Group under the auspices of Department of Health and Human Services Task Force on Alzheimer's Disease. *Neurology* 1984; 34: 939–944.
12. Talairach J, Tournoux P. *Co-Planar Stereotaxic Atlas of the Human Brain*. New York; Thieme Medical Publishers, 1988.
13. Lancaster JL, Summerlin JL, Rainey L, Freitas CS, Fox PT. The Talairach Daemon, a database server for Talairach Atlas Labels. *Neuroimage* 1997; 5: S633.
14. Lancaster JL, Woldorff MG, Parsons LM, Liotti M, Freitas CS, Rainey L, et al. Automated Talairach Atlas labels for functional brain mapping. *Human Brain Mapping* 2000; 10: 120–131.
15. Lancaster JL, Rainey LH, Summerlin JL, Freitas CS, Fox PT, Evans AE, et al. Automated Labeling of the Human Brain: A Preliminary Report on the Development and Evaluation of a Forward-Transform Method. *Human Brain Mapping* 1997; 5: 238–242.
16. Minoshima S, Ficaro EP, Frey KA, Koeppe RA, Kuhl DE. Data Extraction from Brain PET Images Using Three-Dimensional Stereotactic Surface Projections. In: *Quantitative Functional Brain Imaging with Positron Emission Tomography*. Carson RE, Herscovitch P, Daube-Witherspoon ME (eds), San Diego; Academic Press, 1998: 133–137.